Journal of the Meteorological Society of Japan, Vol. 93, No. 4, pp. 477−487, 2015
DOI:10.2151/jmsj.2015-031

An Analytical Solution of Nocturnal Low Level Jets

Sakie HIRA

Climate Prediction Division, Japan Meteorological Agency, Tokyo, Japan

and

Hirotada KANEHISA

Meteorological College, Kashiwa, Japan

(Manuscript received 21 August 2014, in final form 18 May 2015)

Abstract

In this study, an analytical solution of nocturnal low level jets (LLJs) is presented. The present model is an extension of Blackadar, who described the nocturnal LLJ as a result of an inertial oscillation.

In the present model, the momentum equation in the daytime atmospheric boundary layer includes a term representing convective mixing in addition to mixing with a constant diffusion coefficient.

With the convective mixing, the daytime equilibrium wind velocity becomes vertically more uniform than the Ekman solution. In the nighttime atmospheric boundary layer, the convective mixing is assumed to be absent and the diffusion coefficient, which is assumed to be a constant, is smaller than that in the daytime. Without the convective mixing, the nighttime equilibrium wind velocity is the same as that of the Ekman solution.

The analytical solution describes the temporal evolution of nighttime wind velocity as a damped inertial oscillation around the nighttime equilibrium wind velocity, starting from daytime equilibrium wind velocity.

By appropriately selecting the values of parameters in the analytical solution, some previously published results are reproduced. For example, the height of maximum wind speed decreases as time goes on. There exist backward inertial oscillations in addition to the well-known forward inertial oscillations. In the lower levels, the oscillations are rapidly damped.

Keywords nocturnal low level jets; inertial oscillation; atmospheric boundary layer

1. Introduction

During nighttime, and if certain several conditions are met, for example, relatively flat terrain, moderately strong and steady horizontal pressure gradient, and clear sky conducive to strong radiative cooling, supergeostrophic winds blow in the atmospheric boundary layer. This is called the nocturnal low level jet (LLJ). Although the LLJ is a phenomenon in the atmospheric boundary layer, it has an influence on weather. For example, usually the LLJ, if it occurs, is southerly, and hence, it advects warm and moist air. This may be a factor to generate and maintain convective systems resulting in heavy rain.

Blackadar (1957) explained the LLJ as a result of an inertial oscillation (see Fig.1). At sunset, the daytime wind velocity is assumed to be in equilibrium such that the Coriolis, pressure gradient, and turbulent frictional forces are balanced. After sunset (and

Corresponding author: Sakie Hira, Climate Prediction Division, Japan Meteorological Agency, 1-3-4, Otemachi, Chiyoda-ku, Tokyo 100-8122, Japan
E-mail: s-hira@met.kishou.go.jp

before the following sunrise), the frictional force is assumed to vanish above the nocturnal inversion. The force imbalance causes the inertial oscillation of wind velocity starting from the daytime equilibrium wind velocity. Because of the oscillation around the geostrophic wind velocity, the nighttime wind becomes supergeostrophic some time between the sunset and the following sunrise. Although other factors such as blocking and terrain effects (e.g., Wexler 1961; Holton 1967; Jiang et al. 2007; Du and Rotunno 2014) may be at work, Blackadar's (1957) mechanism is believed to be one of the main factors for the LLJ.

Shapiro and Fedorovich (2010) analytically solved the LLJ problem under the following assumptions. The turbulent friction is expressed as diffusion. The diffusion coefficient in the nighttime, which is assumed to be constant, is smaller than that in the daytime. By the method of Laplace transform, they obtained the analytical solution for the nighttime wind velocity. The solution shows a damped inertial oscillation around the nighttime equilibrium wind velocity, starting from the daytime equilibrium wind velocity. The solution shows several characteristic features of LLJs. For example, the height of maximum wind speed deceases with time.

The daytime equilibrium wind velocity in Shapiro and Fedorovich (2010) is the Ekman solution. As is well-known, the angle between the Ekman solution and the geostrophic wind velocity at the ground is 45°, which is rather large compared with that in some observations and numerical simulations (e.g., Grisogono 2011; Holtslag et al. 2013). In addition, usually the daytime equilibrium wind profile is vertically more uniform than the Ekman solution (e.g., Baas et al. 2012). Not only Shapiro and Fedorovich (2010) but also several other analytical studies on LLJs usually assume the diffusion for the turbulent friction (e.g., Sheih 1972). However, as long as diffusion is assumed, even if the vertical dependence of the diffusion coefficient is considered, the vertical uniformity of the daytime equilibrium wind velocity cannot be represented (see Section 2).

Van de Wiel et al. (2010) presented a semi-analytical solution of the LLJ, which is extremely simple in comparison to the rather complicated solution of Shapiro and Fedorovich (2010). Van de Wiel et al. (2010) replaced the nighttime turbulent friction in the momentum equation with the equilibrium counterpart, for the nighttime momentum equation to be easily solved to give a simple solution. Although the solution shows the temporal evolution of nighttime wind velocity compatible with observations, the initial

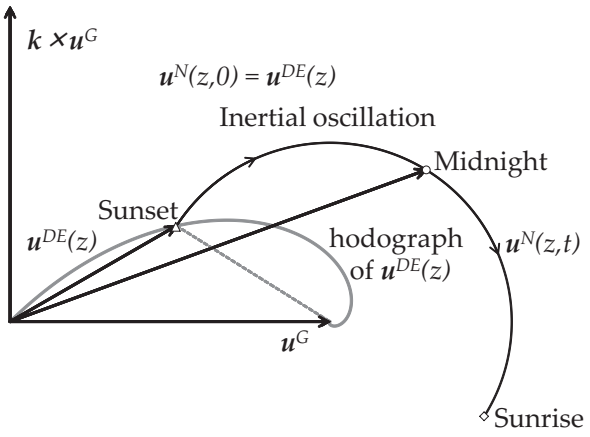

Fig. 1. Schematic of the inertial oscillation of the nighttime wind velocity $\boldsymbol{u}^N(z, t)$. z and t are height and temporal coordinates, respectively. $\boldsymbol{u}^G$ is the geostrophic wind velocity, $\boldsymbol{k}$ is the unit vector pointing vertically upwards. $\boldsymbol{u}^{DE}(z)$ is the daytime equilibrium wind velocity.

value (i.e., the daytime equilibrium wind velocity) is taken from the observations, and not derived in the model. In addition, by the replacement of the turbulent friction with the equilibrium counterpart, the temporal evolution of nighttime wind velocity becomes an undamped inertial oscillation, instead of a damped inertial oscillation, which may be regarded as a usual case. For example, the numerical simulation based on composite data in Baas et al. (2012) shows a damped inertial oscillation. The damping of oscillation becomes conspicuous as the level decreases, although therein the rapid damping at the lowermost level is explained to be caused by the evening transition.

Schröter et al. (2013) considered a mixed layer model of the daytime atmospheric boundary layer. They investigated the relation between the surface friction and the mean wind velocity. In the convective limit, the surface stress is linearly dependent on the mean wind velocity. The linearity represents the convective contribution to friction. While in the neutral limit, the dependence becomes quadratic. This is because the shear velocity feedback must be considered. The quadraticity represents the shear-induced contribution to friction. Schröter et al. (2013) showed that the stress velocity relation can be well approximated by a simple linear combination of the above two limits.

In this study, we present an analytical solution of the LLJ. Taking a hint from Schröter et al. (2013), we

introduce a term representing convective mixing in addition to a mixing with a constant diffusion coefficient in the momentum equation. Due to the convective mixing, the daytime equilibrium wind velocity is vertically more uniform than the Ekman solution. Assuming the absence of convective mixing, we analytically solve the nighttime momentum equation. The obtained solution of nighttime wind velocity shows a damped inertial oscillation around the nighttime equilibrium wind velocity, starting from the daytime equilibrium wind velocity. The nighttime equilibrium wind velocity is the Ekman solution with a reduced diffusion coefficient. By appropriately selecting the values of the parameters, the solution can represent several characteristic features of the LLJ, for example, backward inertial oscillations in addition to the well-known forward inertial oscillations (e.g., Baas et al. 2012). Approximately, the solution of forward inertial oscillation evolves toward the geostrophic wind velocity. On the other hand, the solution of backward inertial oscillation evolves in the opposite direction.

This paper is organized as follows. In Section 2, a term of convective mixing is introduced in the momentum equation. In Section 3, the daytime and nighttime equilibrium wind velocities are derived. In Section 4, the nighttime momentum equation is solved, and the analytical expression of nighttime wind velocity is derived. In Section 5, by appropriately selecting the values of parameters in the solution, some of the previously published results are qualitatively reproduced. In Section 6, concluding remarks are given.

2. Momentum equation

The usual horizontal momentum equation in the atmospheric boundary layer is as follows:

$$\frac{\partial \boldsymbol{u}}{\partial t} = -\frac{1}{\rho}\nabla p - f\boldsymbol{k}\times\boldsymbol{u} + \frac{\partial}{\partial z}\left(K\frac{\partial \boldsymbol{u}}{\partial z}\right), \tag{1}$$

Where $\boldsymbol{u} = \boldsymbol{u}(z, t)$ is the horizontally uniform horizontal wind velocity, z and t are the vertical and temporal coordinates, respectively, ρ is the density, p is the pressure, and $\boldsymbol{k}$ is the unit vector pointing vertically upwards. The Coriolis parameter f is assumed to be constant. The pressure gradient force $-\frac{1}{\rho}\nabla p$ is assumed to be equal to that in the free atmosphere, which is in geostrohic balance, that is, $-\frac{1}{\rho}\nabla p = f\boldsymbol{k}\times\boldsymbol{u}^G$. The geostrophic wind velocity $\boldsymbol{u}^G$ is assumed to be constant. The momentum Eq. (1) can be written in the complex form as

$$\frac{\partial U}{\partial t} = ifU^G - ifU + \frac{\partial}{\partial z}\left(K\frac{\partial U}{\partial z}\right), \tag{2}$$

Where i is the imaginary unit, $U = u + iv$, and u and v are the eastward and northward components of $\boldsymbol{u}$, respectively.

The equilibrium wind velocity is the steady solution of (2) under the boundary conditions $U(0) = 0$ and $\lim_{z\to\infty} U(z) = U^G$. In the case of constant K, this is the Ekman solution $U^{Ekm} = U^{Ekm}(z)$,

$$U^{Ekm}(z) = \left\{1 - \exp\left(-(1+i)\sqrt{\frac{f}{2K}}z\right)\right\}U^G. \tag{3}$$

The Ekman solution U^{Ekm} in (3) depends on z only in the form of $\sqrt{\frac{f}{2K}}z$. Consequently, the form of hodograph of U^{Ekm}, which is the Ekman spiral, does not change for any K, except that U^{Ekm} shifts toward the geostrophic wind velocity U^G as K increases.

The daytime equilibrium wind velocity $U^{DE} = U^{DE}(z)$ is not adequately described in terms of the Ekman solution U^{Ekm} because U^{DE} is usually vertically more uniform than U^{Ekm}, as mentioned in Section 1. We examine whether the vertical uniformity can be represented considering the vertical dependence of the diffusion coefficient K. For a general $K = K(z)$, we cannot analytically obtain the equilibrium wind velocity $U^E = U^E(z)$, which is the steady solution of (2). However, the WKB approximate solution exists for a slowly varying K (see, e.g., Grisogono 2011),

$$U^E(z) = \left\{1 - \left(\frac{K(z)}{K(0)}\right)^{\frac{1}{4}}\exp\left(-(1+i)\sqrt{\frac{f}{2}}\int_0^z \frac{d\xi}{\sqrt{K(\xi)}}\right)\right\}U^G. \tag{4}$$

The typical diffusion coefficient $K(z)$ first monotonically increases near the ground and thereafter monotonically decreases (e.g., Grisogono 2011). From the factor $\frac{1}{\sqrt{K(\xi)}}$ in (4), we may expect that the approximate solution U^E in (4) shifts toward the geostrophic wind velocity U^G in the region where $K(z)$ monotonically decreases, compared with the Ekman solution U^{Ekm} with a constant diffusion coefficient K, which is some average of $K(z)$. This is indeed

the case (see Fig. 2). In Fig. 2, an analytically tractable $K(z)=\{a(z-z_m)^2+b\}^{-2}$ is assumed because the specific form of $K(z)$ for seeing how the Ekman solution with a constant K is qualitatively modified by the slowly varying $K(z)$ does not matter. Here, $a=\left(\frac{1}{\sqrt{K(0)}}-\frac{1}{\sqrt{K(z_m)}}\right)\frac{1}{z_m^2}$, $b=\frac{1}{\sqrt{K(z_m)}}$, and z_m is the level at which $K(z)$ is maximum.

Hence, if U^E becomes nearly uniform, the uniform wind velocity is expected to be equal to the geostrophic wind velocity U^G. This is incompatible with observations. This is the case not only for a slowly varying $K = K(z)$ but also for a general $K = K(z)$, as is easily seen from (2). Indeed, from (2) the equilibrium wind velocity U^E satisfies

$$0=ifU^G-ifU^E+\frac{\partial}{\partial z}K(z)\frac{\partial U^E}{\partial z}. \tag{5}$$

If U^E is nearly uniform in some region $z_1 < z < z_2$, then the diffusion term $\frac{\partial}{\partial z}K(z)\frac{\partial U^E}{\partial z}$ in (5) is small there. This implies that $U^E \approx U^G$ there. Therefore, we can conclude that as long as diffusion for the turbulent friction is assumed, the vertical uniformity of daytime equilibrium wind velocity cannot be represented.

To derive a daytime equilibrium wind velocity $U^{DE} = U^{DE}(z)$ which is vertically more uniform than the Ekman solution, getting a hint from Schröter et al. (2013), we introduce a term representing convective mixing in the momentum Eq. (2) with K being assumed to be constant,

$$\frac{\partial U}{\partial t}=ifU^G-ifU+K\frac{\partial^2 U}{\partial z^2}-f\alpha(U-\bar{U}). \tag{6}$$

The last term on the right hand side of (6) is the convective mixing term. The convective mixing coefficient α is nondimensionalized by the Coriolis parameter f, and $\bar{U}$ is the vertical average of U, i.e., $\bar{U}=\frac{1}{H}\int_0^H dzU$, where H is the depth of the atmosphric boundary layer that is assumed to be constant. The term implies that the wind velocity U is forced to approach the vertical average $\bar{U}$.

The daytime equilibrium wind velocity $U^{DE} = U^{DE}(z)$ is the steady solution of (6) under the boundary conditions $U^{DE}(0) = 0$ and $U^{DE}(H) = U^G$,

$$0=ifU^G-ifU^{DE}+K\frac{\partial^2 U^{DE}}{\partial z^2}-f\alpha\left(U^{DE}-\bar{U}^{DE}\right). \tag{7}$$

Taking the vertical average of (7) gives

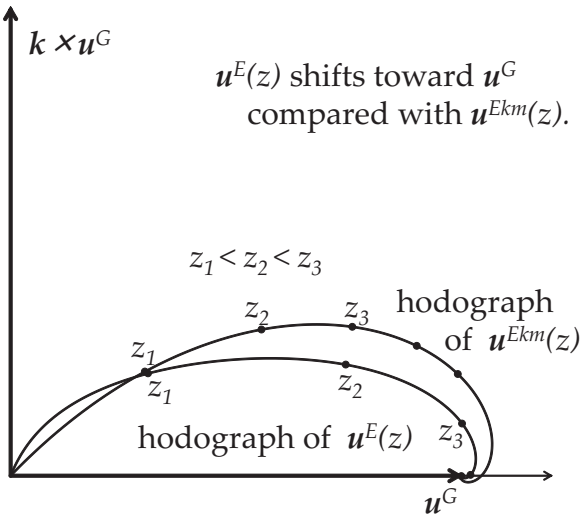

Fig. 2. Example of the hodograph of the equilibrium wind velocity $\boldsymbol{u}^E(z)$ with a slowly varying $K(z)$. $\boldsymbol{u}^G$ is the geostrophic wind velocity, $\boldsymbol{k}$ is the unit vector pointing vertically upwards. $\boldsymbol{u}^{Ekm}(z)$ is the Ekman solution. A profile $K(z) = \{a(z - z_m)^2 + b\}^{-2}$ is assumed, where $a = \left(\frac{1}{\sqrt{K(0)}}-\frac{1}{\sqrt{K(z_m)}}\right)\frac{1}{z_m^2}$, $b=\frac{1}{\sqrt{K(z_m)}}$, $K(0) = 50$ m^2 s^{-1}, $K(z_m) = 60$ m^2 s^{-1} and $z_m = 150$ m.

$$0=ifU^G-if\bar{U}^{DE}+K\frac{1}{H}\left\{\left(\frac{\partial U^{DE}}{\partial z}\right)_{z=H}-\left(\frac{\partial U^{DE}}{\partial z}\right)_{z=0}\right\}. \tag{8}$$

If the depth H is infinite, then the last term on the right hand side of (8) vanishes, and $\bar{U}^{DE}$ becomes equal to U^G. The vertical average of observed daytime winds is different from that of the geostrophic wind. In general, the magnitude of observed daytime winds is much smaller than that of the geostrophic wind. Hence, to obtain $\bar{U}^{DE}$ with $|\bar{U}^{DE}| << |U^G|$, we assume that the depth H is finite.

Multiplying (6) by U^* and taking the real part affords

$$\begin{aligned}\frac{\partial}{\partial t}\left(\frac{|U|^2}{2}\right)=&-f\,\mathrm{Im}\left[U^*U^G\right]-K\left|\frac{\partial U}{\partial z}\right|^2-f\alpha|U-\bar{U}|^2\\&+K\frac{\partial}{\partial z}\left(|U|\frac{\partial|U|}{\partial z}\right)-f\alpha\,\mathrm{Re}\left[\bar{U}^*(U-\bar{U})\right],\end{aligned} \tag{9}$$

where the asterisk $*$ denotes the complex conjugate, and Im and Re denote the imaginary and real parts, respectively. Vertically integrating (9), and noticing

$U(0) = 0$ and $\int_0^H dz(U-\bar{U}) = 0$, we obtain the following energy equation:

$$\frac{d}{dt}\int_0^H dz\frac{|U|^2}{2} = -f\int_0^H dz\,\mathrm{Im}\left[U^*U^G\right] + K\left(|U|\frac{\partial|U|}{\partial z}\right)_{z=H} - K\int_0^H dz\left|\frac{\partial U}{\partial z}\right|^2 - f\alpha\int_0^H dz|U-\bar{U}|^2. \quad (10)$$

The first term on the right hand side of (10) represents the work done by the external force. The second term represents the transport of energy from above. The third and fourth terms, which are negative definite, represent the turbulent dissipation of energy. The negativity implies that the convective mixing term introduced in (6) indeed represents the energy dissipation as required for friction.

3. Equilibrium wind

The daytime equilibrium wind velocity $U^{DE} = U^{DE}(z)$ is the solution of (7) under the boundary conditions $U^{DE}(0) = 0$ and $U^{DE}(H) = U^G$. First, we rewrite (7) as

$$\frac{\partial^2 U^{DE}}{\partial z^2} - \frac{(\alpha+i)f}{K}U^{DE} = -\frac{if}{K}U^G - \frac{\alpha f}{K}\bar{U}^{DE} \quad (11)$$

and solve (11) for $U^{DE}(z)$ in terms of $\bar{U}^{DE}$ and U^G to give

$$U^{DE}(z) = \frac{1}{e^{\beta H}-e^{-\beta H}}\left\{\frac{U^G}{\alpha+i}\left(\alpha+ie^{-\beta H}\right) - \frac{\alpha\bar{U}^{DE}}{\alpha+i}\left(1-e^{-\beta H}\right)\right\}e^{\beta z} + \frac{1}{e^{\beta H}-e^{-\beta H}}\left\{-\frac{U^G}{\alpha+i}\left(\alpha+ie^{\beta H}\right) + \frac{\alpha\bar{U}^{DE}}{\alpha+i}\left(1-e^{\beta H}\right)\right\}e^{-\beta z} + \frac{i}{\alpha+i}U^G + \frac{\alpha}{\alpha+i}\bar{U}^{DE}, \quad (12)$$

Where $\beta = \sqrt{\frac{(\alpha+i)f}{K}}$. Second, taking the vertical average of (12) and neglecting $e^{-\beta H}$ compared with 1 ($|e^{-\beta H}| \ll 1$ for realistic values of f, K, H) gives the vertical average of $U^{DE}(z)$,

$$\bar{U}^{DE} = \frac{\alpha - i + i\beta H}{2\alpha + i\beta H}U^G. \quad (13)$$

Finally, substituting (13) into (12) and neglecting $e^{-\beta H}$ compared with 1 gives the daytime equilibrium wind velocity U^{DE},

$$U^{DE}(z) = \left(1-e^{-\beta z}\right)U^G - \left(2+\frac{i\beta H}{\alpha}\right)^{-1}\left\{1-e^{-\beta z}-e^{-\beta(H-z)}\right\}U^G. \quad (14)$$

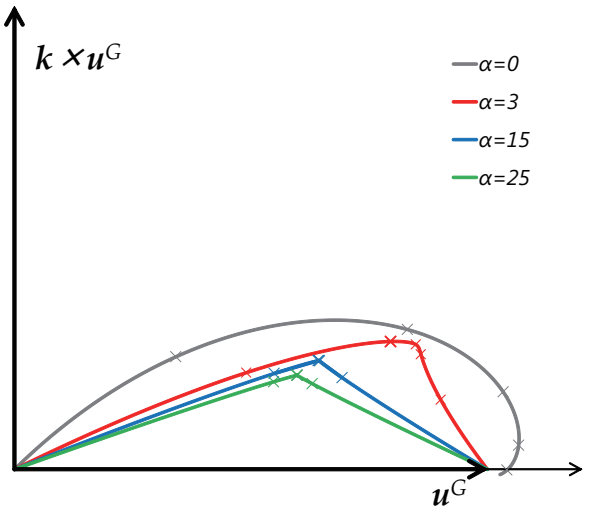

Fig. 3. The hodograph of the daytime equilibrium wind velocity in (14). $f = 1 \times 10^{-4}$ s^{-1}, $K = 1$ m^2 s^{-1}, $H = 500$ m. Crosses (×) indicate $z = \frac{nH}{10}$ ($n = 1, 3, 5, 7, 9$). For $\alpha = 15$ and $\alpha = 25$, the three crosses ($n = 3, 5, 7$) overlap because of the vertical uniformity.

In the limit of $\alpha \to 0$, the daytime equilibrium wind velocity in (14) becomes essentially the Ekman solution although the depth H is finite instead of infinite,

$$\lim_{\alpha\to 0} U^{DE}(z) = \left(1-e^{-\beta_0 z}\right)U^G, \quad (15)$$

Where $\beta_0 = \sqrt{\frac{if}{K}}$. While in the limit of $\alpha \to \infty$, the daytime equilibrium wind velocity in (14) becomes vertically uniform except that $U^{DE}(0) = 0$ and $U^{DE}(H) = U^G$,

$$\lim_{\alpha\to\infty} U^{DE}(z) = \frac{1}{2}U^G \quad \text{for} \quad 0 < z < H. \quad (16)$$

Of course, the limiting case ($\alpha \to \infty$) is never realized, an idealized case.

The hodograph of $U^{DE}(z)$ in (14) is depicted for $f = 1 \times 10^{-4}$ s^{-1}, $K = 1$ m^2 s^{-1}, $H = 500$ m, and for several values of α in Fig. 3 (the component representation

of wind velocity is given in Appendix). The greater α is, the more uniform $U^{DE}(z)$ is in the vertical and the smaller the ageostrophic angle at the ground, although the discontinuity in tangent of the hodograph is unrealistic.

Since the convective mixing is suppressed after the sunset (and before the following sunrise), the convective mixing coefficient α is assumed to vanish in the nighttime. Then, the nighttime equilibrium wind velocity $U^{NE} = U^{NE}(z)$ is given by (15) but with a reduced nighttime diffusion coefficient $\tilde{K}(< K)$,

$$U^{NE}(z) = \left(1 - e^{-\tilde{\beta}_0 z}\right) U^G, \tag{17}$$

Where $\tilde{\beta}_0 = \sqrt{\dfrac{if}{\tilde{K}}}$.

4. Nocturnal wind

We assume that the daytime wind velocity becomes the equilibrium wind velocity $U^{DE}(z)$ by sunset (t = 0). Because of the absence of the convective mixing $\alpha = 0$, the nighttime wind velocity $U^N = U^N(z, t)$ is the solution of

$$\frac{\partial U^N}{\partial t} = ifU^G - ifU^N + \tilde{K}\frac{\partial^2 U^N}{\partial z^2} \tag{18}$$

under the boundary conditions $U^N(0, t) = 0$ and $U^N(H, t) = U^G$, and the initial condition $U^N(z, 0) = U^{DE}(z)$, which is derived in Section 3 by the introduction of the convective mixing $\alpha > 0$ and is vertically more uniform than the Ekman solution. While, the nighttime equilibrium wind velocity $U^{NE} = U^{NE}(z)$ is the solution of

$$0 = ifU^G - ifU^{NE} + \tilde{K}\frac{\partial^2 U^{NE}}{\partial z^2} \tag{19}$$

under the boundary conditions $U^{NE}(0) = 0$ and $U^{NE}(H) = U^G$. In the absence of the convective mixing $\alpha = 0$, the nighttime equilibrium wind velocity $U^N = U^{NE}(z)$ is essentially the same as the Ekman solution. We define $U^I(z, t)$ as

$$U^N(z,t) = U^{NE}(z) + e^{-ift}U^I(z,t). \tag{20}$$

Then, from (18), (19), and (20), $U^I(z, t)$ is the solution of

$$\frac{\partial U^I}{\partial t} = \tilde{K}\frac{\partial^2 U^I}{\partial z^2} \tag{21}$$

under the boundary and initial conditions,

$$\begin{aligned} &U^I(0,t) = 0,\ U^I(H,t) = 0, \\ &U^I(z,0) = U^{DE}(z) - U^{NE}(z). \end{aligned} \tag{22}$$

Although $U^I(z, t)$ is defined only in the region $0 \le z \le H$, we regard $U^I(z, t)$ as an antisymmetric function with respect to z in the region $-H \le z \le H$,

$$U^I(z,t) = -U^I(-z,t) \quad \text{for} \quad -H \le z \le 0,$$

and further as a periodic function with respect to z with a period $2H$ in the region $-\infty < z < \infty$.

$$U^I(z+2H,t) = U^I(z,t).$$

Then, we can expand $U^I(z, t)$ in terms of trigonometric functions as

$$U^I(z,t) = \sum_{m=1}^{\infty} S_m(t)\sin\frac{m\pi z}{H}. \tag{23}$$

Because of the boundary conditions in (22), which imply that $U^I(z, t)$ is continuous up to the first derivative at z = 0, H, the infinite sum $\sum_{m=1}^{\infty}$ in (23) can be well approximated by a finite sum $\sum_{m=1}^{M}$ (we take M = 100 in Section 5).

By the substitution of (23) into (21), the temporal dependence of $S_m(t)$ is determined,

$$S_m(t) = S_m(0)\exp\left(-\tilde{K}\left(\frac{m\pi}{H}\right)^2 t\right). \tag{24}$$

By the integration of (23) with respect to z at t = 0, the functional dependence of $S_m(0)$ on $U^I(z, 0)$ is determined,

$$S_m(0) = \frac{2}{H}\int_0^H dz U^I(z,0)\sin\frac{m\pi z}{H}. \tag{25}$$

From the initial condition in (22), $U^I(z, 0)$ = $U^{DE}(z)$ – $U^{NE}(z)$. Substituting (14) and (17) into $U^I(z, 0)$, performing the integration in (25), and neglecting $e^{-\beta H}$ and $e^{-\tilde{\beta}_0 H}$ compared with 1 affords $S_m(0) = \dfrac{2}{H} I_m$, where

$$\begin{aligned} I_m = &\left[\frac{\mu}{\mu^2 + \tilde{\beta}_0^2} - \frac{\mu}{\mu^2 + \beta^2}\right. \\ &\left. - \left\{1 - (-1)^m\right\}\left(2 + \frac{i\beta H}{\alpha}\right)^{-1}\left(\frac{1}{\mu} - \frac{\mu}{\mu^2 + \beta^2}\right)\right] U^G, \end{aligned} \tag{26}$$

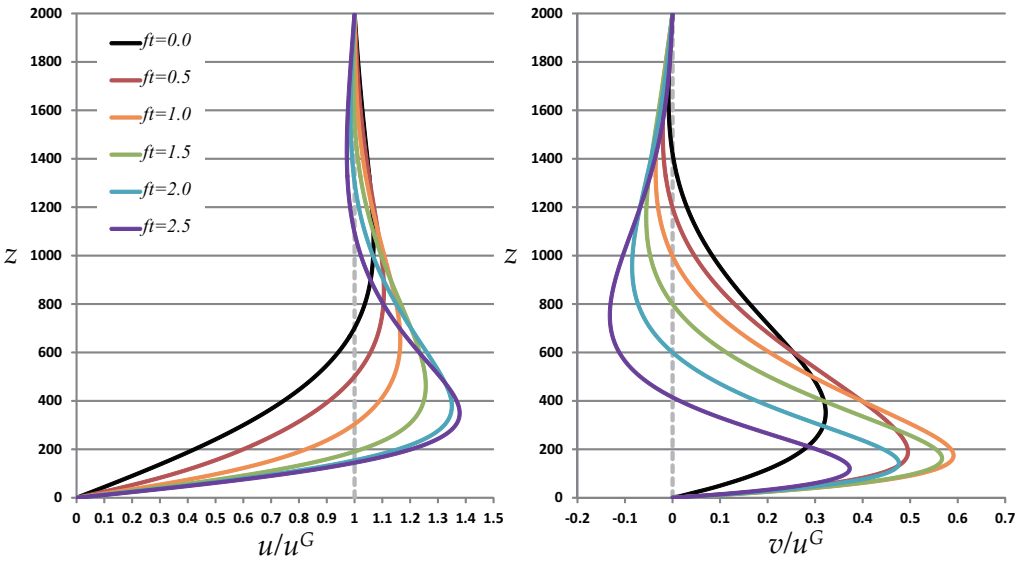

Fig. 4. The temporal evolution of the vertical profile of the nighttime wind velocity in (27). $f = 1 \times 10^{-4}$ s^{-1}, $K = 10$ m^2 s^{-1}, $\tilde{K} = 1$ m^2 s^{-1}, $\alpha = 0$, $H = 2000$ m. The left and right panels depict the components parallel and perpendicular to the geostrophic wind velocity, respectively.

and $\mu = \dfrac{m\pi}{H}$. From (20), (23), and (24), we obtain the nighttime wind velocity $U^N(z,t)$,

$$U^N(z,t) = U^{NE}(z) + e^{-ift}\frac{2}{H}\sum_{m=1}^{\infty} I_m e^{-\tilde{K}\left(\frac{m\pi}{H}\right)^2 t}\sin\frac{m\pi z}{H}, \tag{27}$$

where I_m is given by (26). As is evident in (27), the nighttime wind velocity $U^N(z, t)$ shows a damped inertial oscillation around the nighttime equilibrium wind velocity $U^{NE}(z)$.

5. Examples

To assess the validity of the solution in (27), we try to reproduce some of the previously published results by appropriately selecting the values of the parameters.

Shapiro and Fedrovich (2010) analytically obtained the nighttime wind velocity under the assumptions that both the daytime and nighttime equilibrium wind velocities are the Ekman solutions with the nighttime diffusion coefficient smaller than that with the daytime. To reproduce their results, we take $f = 1 \times 10^{-4}$ s^{-1}, $K = 10$ m^2 s^{-1}, $\tilde{K} = 1$ m^2 s^{-1} $\alpha = 0$, and $H = 2000$ m in the solution (27), and show the temporal evolution of the vertical profile of the nighttime wind velocity $U^N(z, t)$ in Fig. 4. On the left panel of Fig. 4, the component along the geostrophic wind velocity is depicted, and on the right panel, the component perpendicular to it is depicted. The level of the maximum wind speed descends as time goes on. This is partly compatible with some observations (e.g., Bonner 1968; Mitchell et al. 1995). Their results are qualitatively well reproduced (see Fig. 2 in Shapiro and Fedorovich 2010).

Baas et al. (2012) presented the numerically simulated hodographs of nighttime wind velocity based on their composite data. To reproduce their result, we take $f = 1 \times 10^{-4}$ s^{-1}, $K = 0.88$ m^2 s^{-1}, $\tilde{K} = 0.22$ m^2 s^{-1}, $\alpha = 15$, and $H = 1000$ m in the solution (27), and show the hodographs of the nigttime wind velocity $U^N(z, t)$ in Fig. 5. There exist backward inertial oscillations in the lower levels in addition to forward inertial oscillations in the upper levels. The lowermost oscillation is damped rapidly. Their results are at least qualitatively well reproduced (see Fig. 4 in Baas et al. 2012) although they attributed the rapid damping to the evening transition.

Finally, we try to reproduce the observed hodographs in Van de Wiel et al. (2010), whose damping is weak. We take $f = 1.15 \times 10^{-4}$ s^{-1}, $K = 1$ m^2 s^{-1}, $\tilde{K} = 0.1$ m^2 s^{-1}, $\alpha = 15$, and $H = 500$ m in the solution (27), and show the hodographs of the nighttime wind velocity $U^N(z, t)$ in Fig. 6. Their results are, we think, at least qualitatively reproduced (see Fig. 8 in

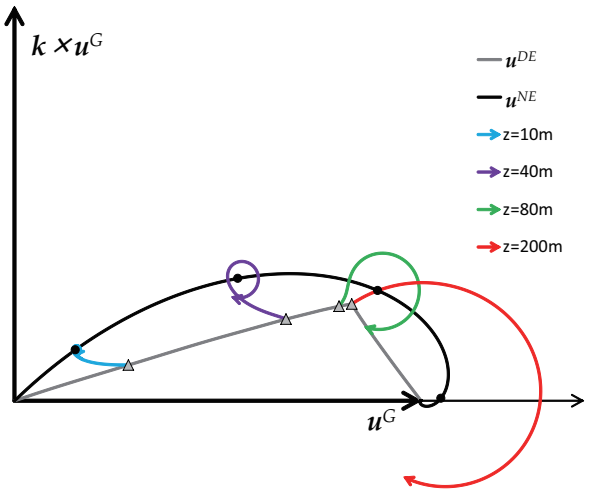

Fig. 5. The hodographs of the nighttime wind velocity in (27). $f = 1 \times 10^{-4}$ s^{-1}, $K = 0.88$ m^2 s^{-1}, $\tilde{K} = 0.22$ m^2 s^{-1}, $\alpha = 15$, $H = 1000$ m. Triangles (△) mark the daytime equilibrium wind velocity.

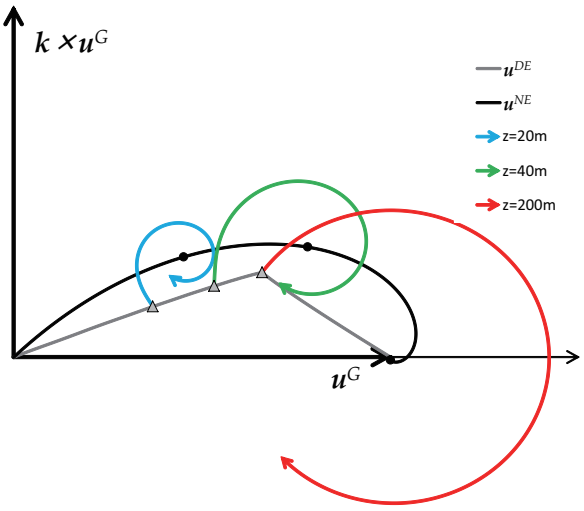

Fig. 6. The hodographs of the nighttime wind velocity in (27). $f = 1.15 \times 10^{-4}$ s^{-1}, $K = 1$ m^2 s^{-1}, $\tilde{K} = 0.1$ m^2 s^{-1}, $\alpha = 15$, $H = 500$ m. Triangles (△) mark the daytime equilibrium wind velocity.

Van de Wiel et al. 2010).

6. Concluding remarks

In the usual analytical studies on the atmospheric boundary layer, the turbulent friction is parameterized as diffusion. In the case of a constant diffusion coefficient, the equilibrium wind velocity is given by the Ekman solution. The angle θ_0 between the Ekman solution and the geostrophic wind velocity at the ground is 45°, which is rather large compared with some observations and/or numerical simulations. In addition, the vertical profile of daytime equilibrium wind velocity is usually more uniform in the vertical than the Ekman solution. Considering the vertical dependence of the diffusion coefficient, we can reduce the angle θ_0 to a realistic value (e.g., Grisogono 2011). However, the vertical uniformity cannot result even if the vertical dependence of the diffusion coefficient is counted.

Taking a hint from Shröter et al. (2013), we introduced a term representing convective mixing in the horizontal momentum equation in the daytime atmospheric boundary layer, so that the turbulent friction is represented as a linear combination of convective mixing and diffusion. Due to the convective mixing, the daytime equilibrium wind velocity becomes vertically more uniform than the Ekman solution. Assuming that the convective mixing is absent and that the diffusion coefficient is reduced in the nighttime, we analytically solved the momentum equation. The obtained solution of nighttime wind velocity shows a damped inertial oscillation around the nighttime equilibrium wind velocity, starting from a daytime equilibrium wind velocity. By appropriately selecting the values of parameters in the solution, some previously published results are qualitatively reproduced, although the height H of the boundary layer is not derived in the model but is also a prescribed parameter, which is a limitation of the present model. The reproducibility implies that it has some validity to parameterize the turbulent friction by the linear combination of diffusion and convective mixing.

In this study, we assumed that the daytime wind velocity has become the equilibrium wind velocity by sunset. However, unless the turbulent friction is too strong, the daytime wind velocity may inertially oscillate (e.g., Thorpe and Guymer 1977). In midlatitudes near 30°N, the frequency f of the inertial oscillation is nearly equal to the angular frequency of the earth, that is, nearly equal to the frequency of the diurnal heating. Because of this, the resonance between the diurnal heating and the inertial oscillation may occur (e.g., Shibuya et al. 2014). If the resonance occurs, the daytime wind velocity keeps on inertially oscillating. Furthermore, the amplitude may grow rather than be damped to the equilibrium.

In this study, both the convective mixing coeffi-

cient α and diffusion coefficient K are assumed to be temporally piecewise constant. That is, both α and K are positive constants in the daytime, and α vanishes and K is reduced in the nighttime. To consider the above mentioned resonance effect, we must consider diurnally varying α and K. Although Sheih (1972) analytically studied the case with a diurnal varying diffusion coefficient, he did not consider the resonance. Recently, Shibuya et al. (2014) numerically investigated the resonant inertial oscillation and proposed the mechanism of the resonance. However, the analytical study is still to be conducted.

Analytical investigation of the resonant inertial oscillation with diurnally (and vertically if possible) varying frictional coefficients will be conducted in our future studies. Our model has many difficulties (e.g., constant H, small $e^{-\beta H}$, etc) that need to be overcome to represent the developing convective boundary layer.

Acknowledgments

We thank three anonymous reviewers for their many valuable comments and constructive criticism.

Appendix

1. Component representation of $U^{DE}(z)$

For the presentation simplicity, we set the coordinates axes so that $u^G = |\boldsymbol{u}^G|, v^G = 0$. In this case the complex geostrophic wind velocity becomes $U^G = u^G + iv^G = u^G$, and the daytime equilibrium wind velocity in (3.4) becomes

$$U^{DE}(z) = \left(1 - e^{-\beta z}\right)u^G - \left(2 + \frac{i\beta H}{\alpha}\right)^{-1}\left\{1 - e^{-\beta z} - e^{-\beta(H-z)}\right\}u^G. \tag{A1}$$

We rewrite the parameter β in (A.1) as

$$\beta = \sqrt{\frac{(\alpha + i)f}{K}} = \gamma\left(\frac{1}{\sqrt{\tau}} + i\sqrt{\tau}\right), \tag{A2}$$

Where $\gamma = \sqrt{\frac{f}{2K}}$, $\tau = \tan\frac{\theta}{2}$, and $\theta = \tan^{-1}\frac{1}{\alpha}$. Substituting (A.2) into (A.1) and after some manipulation, we obtain the components of $U^{DE}(z) = u^{DE}(z) + iv^{DE}(z)$,

$$\begin{aligned} u^{DE}(z) &= u^G\left(1 - e^{-\frac{\gamma z}{\sqrt{\tau}}}\cos\sqrt{\tau}\gamma z\right) \\ &\quad - \frac{u^G}{\left(2 - \frac{\gamma H\sqrt{\tau}}{\alpha}\right)^2 + \left(\frac{\gamma H}{\alpha\sqrt{\tau}}\right)^2} \\ &\quad \left[\left(2 - \frac{\gamma H\sqrt{\tau}}{\alpha}\right)\right. \\ &\quad \left\{1 - e^{-\frac{\gamma z}{\sqrt{\tau}}}\cos\sqrt{\tau}\gamma z - e^{-\frac{\gamma(H-z)}{\sqrt{\tau}}}\cos\sqrt{\tau}\gamma(H-z)\right\} \\ &\quad \left. + \frac{\gamma H}{\alpha\sqrt{\tau}}\left\{e^{-\frac{\gamma z}{\sqrt{\tau}}}\sin\sqrt{\tau}\gamma z + e^{-\frac{\gamma(H-z)}{\sqrt{\tau}}}\sin\sqrt{\tau}\gamma(H-z)\right\}\right], \end{aligned}$$

$$\begin{aligned} v^{DE}(z) &= u^G e^{-\frac{\gamma z}{\sqrt{\tau}}}\sin\sqrt{\tau}\gamma z \\ &\quad + \frac{u^G}{\left(2 - \frac{\gamma H\sqrt{\tau}}{\alpha}\right)^2 + \left(\frac{\gamma H}{\alpha\sqrt{\tau}}\right)^2} \\ &\quad \left[\frac{\gamma H}{\alpha\sqrt{\tau}}\right. \\ &\quad \left\{1 - e^{-\frac{\gamma z}{\sqrt{\tau}}}\cos\sqrt{\tau}\gamma z - e^{-\frac{\gamma(H-z)}{\sqrt{\tau}}}\cos\sqrt{\tau}\gamma(H-z)\right\} \\ &\quad - \left(2 - \frac{\gamma H\sqrt{\tau}}{\alpha}\right) \\ &\quad \left. \left\{e^{-\frac{\gamma z}{\sqrt{\tau}}}\sin\sqrt{\tau}\gamma z + e^{-\frac{\gamma(H-z)}{\sqrt{\tau}}}\sin\sqrt{\tau}\gamma(H-z)\right\}\right]. \end{aligned}$$

2. Component representation of $U^{NE}(z)$

The nighttime equilibrium wind velocity in (17) becomes

$$U^{NE}(z) = \left(1 - e^{-\tilde{\beta}_0 z}\right)u^G. \tag{A3}$$

We rewrite the parameter $\tilde{\beta}_0$ in (A.3) as

$$\tilde{\beta}_0 = \sqrt{\frac{if}{\tilde{K}}} = \tilde{\gamma}(1 + i), \tag{A4}$$

Where $\tilde{\gamma} = \sqrt{\frac{f}{2\tilde{K}}}$. Substituting (A.4) into (A.3), we obtain the components of $U^{NE}(z) = u^{NE}(z) + iv^{NE}(z)$,

$$\begin{aligned} u^{NE}(z) &= u^G\left(1 - e^{-\tilde{\gamma}z}\cos\tilde{\gamma}z\right), \\ v^{NE}(z) &= u^G e^{-\tilde{\gamma}z}\sin\tilde{\gamma}z. \end{aligned} \tag{A5}$$

3. Component representation of $U^N(z, t)$

The coefficients I_m in (26) of the nighttime wind velocity $U^N(z, t)$ in (27) becomes

$$I_m = \left[\frac{\mu}{\mu^2 + \tilde{\beta}_0^2} - \frac{\mu}{\mu^2 + \beta^2} - \left\{1 - (-1)^m\right\} \left(2 + \frac{i\beta H}{\alpha}\right)^{-1} \left\{ \frac{1}{\mu} - \frac{\mu}{\mu^2 + \beta^2} \right\} \right] u^G, \tag{A6}$$

where $\mu = \dfrac{m\pi}{H}$, $\beta = \gamma\left(\dfrac{1}{\sqrt{\tau}} + i\sqrt{\tau}\right)$, and $\tilde{\beta}_0 = \tilde{\gamma}(1+i)$. Substituting (A.3), (A.5) and (A.6) into (27) and after some manipulation, we obtain the components of $U^N(z,t) = u^N(z,t) + iv^N(z,t)$,

$$u^N(z,t) = u^G\left(1 - e^{-\tilde{\gamma}z}\cos\tilde{\gamma}z\right) + \frac{2}{H}\sum_{m=1}^{\infty}\left(\mathrm{Re}[I_m]\cos ft + \mathrm{Im}[I_m]\sin ft\right)e^{-t\tilde{K}\mu^2}\sin\mu z,$$

$$v^N(z,t) = u^G e^{-\tilde{\gamma}z}\sin\tilde{\gamma}zn + \frac{2}{H}\sum_{m=1}^{\infty}\left(\mathrm{Im}[I_m]\cos ft - \mathrm{Re}[I_m]\sin ft\right)e^{-t\tilde{K}\mu^2}\sin\mu z,$$

where

$$\mathrm{Re}[I_m] = \left[\mu\left\{ \frac{\mu^2}{\mu^4 + 4\tilde{\gamma}^4} - \frac{\mu^2 + 2\alpha\gamma^2}{(\mu^2 + 2\alpha\gamma^2)^2 + 4\gamma^4} \right\} - \left\{1 - (-1)^m\right\}\left\{ \frac{1}{\mu} - \frac{\mu(\mu^2 + 2\alpha\gamma^2)}{(\mu^2 + 2\alpha\gamma^2)^2 + 4\gamma^4} \right\} \frac{\alpha(2\alpha - \gamma H\sqrt{\tau})}{(2\alpha - \gamma H\sqrt{\tau})^2 + \dfrac{\gamma^2 H^2}{\tau}} - \left\{1 - (-1)^m\right\} \frac{2\mu\gamma^2}{(\mu^2 + 2\alpha\gamma^2)^2 + 4\gamma^4} \frac{\alpha\dfrac{\gamma H}{\sqrt{\tau}}}{(2\alpha - \gamma H\sqrt{\tau})^2 + \dfrac{\gamma^2 H^2}{\tau}} \right] u^G$$

and

$$\mathrm{Im}[I_m] = \left[-2\mu\left\{ \frac{\tilde{\gamma}^2}{\mu^4 + 4\tilde{\gamma}^4} - \frac{\gamma^2}{(\mu^2 + 2\alpha\gamma^2)^2 + 4\gamma^4} \right\} + \left\{1 - (-1)^m\right\}\left\{ \frac{1}{\mu} - \frac{\mu(\mu^2 + 2\alpha\gamma^2)}{(\mu^2 + 2\alpha\gamma^2)^2 + 4\gamma^4} \right\} \frac{\alpha\dfrac{\gamma H}{\sqrt{\tau}}}{(2\alpha - \gamma H\sqrt{\tau})^2 + \dfrac{\gamma^2 H^2}{\tau}} - \left\{1 - (-1)^m\right\} \frac{2\mu\gamma^2}{(\mu^2 + 2\alpha\gamma^2)^2 + 4\gamma^4} \frac{\alpha(2\alpha - \gamma H\sqrt{\tau})}{(2\alpha - \gamma H\sqrt{\tau})^2 + \dfrac{\gamma^2 H^2}{\tau}} \right] u^G.$$

References

Baas, P., B. J. H. Van de Wiel, L. Van den Brink, and A. A. M. Holtslag, 2012: Composite hodographs and inertial oscillations in the nocturnal boundary layer. *Quart. J. Roy. Meteor. Soc.*, **138**, 528–535.

Blackadar, A. K., 1957: Boundary layer wind maxima and their significance for the growth of nocturnal inversions. *Bull. Amer. Meteor. Soc.*, **38**, 283–290.

Bonner, W. D., 1968: Climatology of the low level jet. *Mon. Wea. Rev.*, **96**, 833–850.

Du, Y., and R. Rotunno, 2014: A simple analytical model of the nocturnal low-level jet over the Great plains of the United States. *J. Atmos. Sci.*, **71**, 3674–3683.

Grisogono, B., 2011: The angle of the near-surface wind-turning in weakly stable boundary layers. *Quart. J. Roy. Meteor. Soc.*, **137**, 700–708.

Holton, J. R., 1967: The diurnal boundary layer wind oscillation above sloping terrain. *Tellus A*, **19**, 199–205.

Holtslag, A. A. M., G. Svensson, P. Baas, S.Basu, B. Beare, A. C. M. Beljaars, F. C. Bosveld, J. Cuxart, G. J. Steeneveld, M. Tjernstrom, and B. J. H. van de Wiel, 2013: Stable atmospheric boundary layers and diurnal cycles. *Bull. Amer. Meteor. Soc.*, **94**, 1691–1706.

Jiang, X., N. C. Lau, I. M. Held, and J. J. Ploshay, 2007: Mechanism of the Great Plains low-level jet as simulated in an AGCM. *J. Atmos. Sci.*, **64**, 532–547.

Mitchell, M. J., R. W. Arritt, and K. Labas, 1995: A climatology of the warm season Great Plains low-level jet using wind profiler observations. *Wea. Forcasting*, **10**, 576–591.

Schröter, J. S., A. F. Moene, and A. A. M. Holtslag, 2013: Convective boundary layer wind dynamics and inertial oscillations: the influence of surface stress. *Quart. J. Roy. Meteor. Soc.*, **139**, 1694–1711.

Shapiro, A., and E. Fedorovich, 2010: Analytical description of a nocturnal low-level jet. *Quart. J. Roy. Meteor.*

Soc., **136**, 1255–1262.

Sheih, C. M., 1972: A theoretical study of the diurnal wind variations in the planetary boundary layer. *J. Atmos. Sci.*, **29**, 995–998.

Shibuya, R., K. Sato, and M. Nakanishi, 2014: Diurnal wind cycles forcing inertial oscillations: A latitude-dependent resonance phenomenon. *J. Atmos. Sci.*, **71**, 767–781.

Thorpe, A. J., and T. H. Guymer, 1977: The nocturnal jet. *Quart. J. Roy. Meteor. Soc.*, **103**, 633–653.

Van de Wiel, B. J. H., A. F. Moene, G. J. Steeneveld, P. Baas, F. C. Bosveld, and A. A. M. Holtslag, 2010: A conceptual view on inertial oscillations and nocturnal low-level jets. *J. Atmos. Sci.*, **67**, 2679–2689.

Wexler, H., 1961: A boundary layer interpretation of the low level jet. *Tellus*, **13**, 368–378.